

Faults, Fractures, Formation, and Stress at Fish Lake: Controls on Wellbore-Scale Permeability in a Deep Circulation Geothermal System

Irene Wallis¹, Alex Milton², Zach Brown², Leland Davis², John Casteel³, Brad Peters³

¹ Cubic Earth

² Geologica Geothermal Group

³ Open Mountain Energy

Keywords

Borehole Image, Microresistivity Image, Permeability, Stress

ABSTRACT

The logging and testing programs conducted in three adjacent wells at the Fish Lake Geothermal Project has revealed insight into the stress tensor and the controls on wellbore-scale permeability. The logging program included acquisition of microresistivity borehole images (MBI) and petrophysical logs. The testing program included an extended leak-off test (XLOT) that was successfully conducted using rig pumps, rather than the usual low-rate positive pressure pumps. Detailed relogging of cuttings and a program of well testing are ongoing, with early results included herein. We show that Fish Lake wells are impacted by geometric sample bias, as is expected for all wells. We illustrate fault identification using MBI and propose a novel approach for discerning which faults may be hydraulically meaningful. We share insights on the stress tensor that were generated from MBI and XLOT, and then discuss how borehole deviation impacts the azimuth of drilling induced tensile fractures. The results of this detailed, geothermal-specific, and interdisciplinary borehole analysis improved our understating of geologic controls on permeability at Fish Lake, which is insight that can be applied to future well targets and the conceptual model.

1. Introduction

The Fish Lake Geothermal Project is in Nevada, USA near the town of Dyer (Figure 1). It is currently being evaluated by Open Mountain Energy for power potential. This paper presents an integrated and interdisciplinary approach to microresistivity borehole image (MBI) analysis in three resource delineation wells that were drilled from the same pad, with well names anonymized herein. The results of this study inform our understating of what controls permeability at Fish Lake. We also discuss insight these data provide on the tectonic stress tensor, which is the foundation of future geomechanical modelling studies.

Fish Lake is a deep-circulation type, conventional geothermal system. The stratigraphy at Fish Lake comprises slightly to moderately dipping Tertiary volcanic and sedimentary strata overlying Paleozoic folded and thrust metamorphic basement rocks. The Paleozoic basement at Fish Lake includes meta-arkose, quartzite, phyllite, and marble. At a 1:62,500 scale (i.e., within the valley) the primary structural trends include N-S striking, normal faults (Robinson & Crowder, 1973).

Borehole imaging of conventional geothermal wells is becoming a standard practice. They inform development of local and regional structural models (e.g., Davatzes & Hickman, 2010; McNamara et al., 2019), can be used to constrain the tectonic stress tensor and to model the tendency of fractures to maintain permeability through re-shear (e.g., Barton et al., 1998; Nemčok et al., 2007; Wallis et al., 2020a). When combined with well testing, MBI interpretation can reveal the controls on hydrothermal fluid flux (e.g., Sone et al., 2023, Wallis et al., 2012).

Analysis of MBI acquired in geothermal wells differs from oil and gas. Interpretation of images acquired in geothermal wells must consider the significant thermal stresses at the borehole wall. Thermally enhanced (dominantly tensile) hoop stresses can increase apparent fracture apertures, part discontinuities that are not open in the reservoir, and significantly modify the type and intensity of drilling induced damage. MBI interpretation in geothermal wells must also account for a wide range of mineral fills and rock types.

Our paper starts with a description of methods. There are three areas where our methods differ from other borehole image studies in geothermal wells (e.g., Davatzes & Hickman, 2010; Massiot et al., 2015): (1) we have a geothermal-specific approach to categorizing fractures that accounts for hydrothermal alteration, (2) we quantify geometric sample bias, and (3) we use a novel category of drilling induced damage (interacting tensile fractures). We present the results of our MBI interpretation and an interdisciplinary analysis of these data before focusing on two areas of discussion: (1) the explanatory model for how drilling induced damage rotates around the borehole wall as well inclination/deviation changes and (2) insights that were gained into the controls on wellbore-scale permeability and how they compare to volcanic-hosted, high temperature geothermal wells.

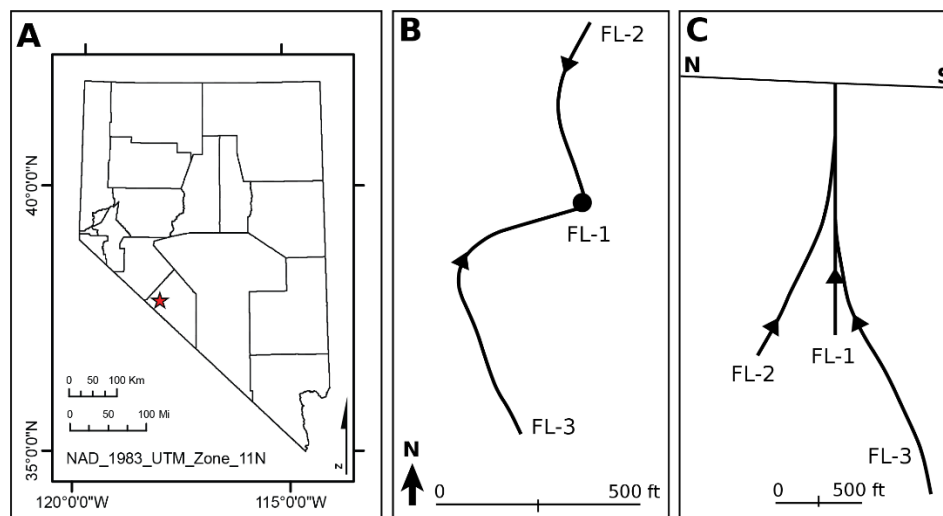


Figure 1: Location of Fish Lake Geothermal Project (A) and the wells included in this study pictured in plan-view (B) and section (C). Triangles on the well paths are production casing shoes.

2. Methods

2.1 Borehole Images and their Interpretation

Fullbore Formation Microscanner (FMI, Schlumberger) MBI were acquired below the production casing shoes in the three wells. Processed, concatenated images were interpreted manually using WellCAD software. Electrically conductive fractures, which may be open (i.e., water filled) or filled with a moderately conductive mineral (e.g., clay), were quantified and are referred to here as ‘non-haloed, conductive fractures’ (NHC-fractures; Figure 2). Each NHC-fracture is categorized as high or low confidence, depending on how well the fracture geometry is constrained.

All features that are likely filled are grouped in this study and referred to as ‘resistive or haloed fractures’ (RH-fractures; Figure 2). There is a range of log responses which indicate that fractures are mineral filled. These include resistive sinusoids (i.e., filled with a resistive mineral), a bright halo along the entire length of a conductive fracture (i.e., current attraction, likely filled with a very conductive mineral like pyrite), or bright halos at the apices of the fracture (i.e., preventing the current from passing, likely a resistive mineral fill). A wide, relatively conductive zone surrounding a fracture is interpreted here as an alteration halo. Given the intensity of alteration required to form a conductive halo, these fractures are likely also to be filled and have been included in the group classified as mineral filled.

An MBI generates a detailed picture of lithologic textures. This contrasts with an acoustic borehole image (ABI) where lithologic variation is only captured if the elastic rock properties and/or borehole surface roughness change with lithology. Textures captured by the Fish Lake MBI include bedding, foliation, and clast arrangements (Figure 2). Graded and sharp contacts are quantified in the image. Representative picks of bedding or foliation are made to capture the overall attitude. Systematic quantification of bedding/foliation from the MBI is an important part of differentiating bedding/foliation from tectonic fractures and discerning what impact the rock fabric has on drilling induced damage.

The relative, apparent aperture of each fracture is quantified because larger fractures are more likely to influence borehole hydrology. In this study, apparent fracture aperture refers to the measurable thickness of a fracture on the MBI, corrected for wellbore deviation. There are two reasons why this apparent aperture is not the actual aperture in the reservoir. First, MBI tools have an ~0.5-inch depth of penetration into the borehole wall, so features perpendicular to the borehole may appear thinner on the image than those at more acute angles. Second, the thermally enhanced hoop stresses present in a geothermal well may increase apparent fracture aperture. Despite these issues, there is likely to be a gross, scaling relationship between apparent aperture picked from the MBI and actual aperture in the reservoir. To appropriately capture this relationship, fracture aperture is reported as six categories that range from very small to very large.

Many borehole image analysis software packages include the Luthi and Souhathié (1990) method for calculating MBI fracture aperture. This method is based on the relationship between the resistivity of the borehole mud, the formation, and the additional current flow generated by the presence of a fracture with a given width (i.e., excess current). The Luthi and Souhathié (1990) method was developed with modelled shallow formation resistivities of 10, 100 and 1000 ohm.m, fracture dips from 0 to 40° (assuming a vertical well), and fracture apertures < 0.2 mm.

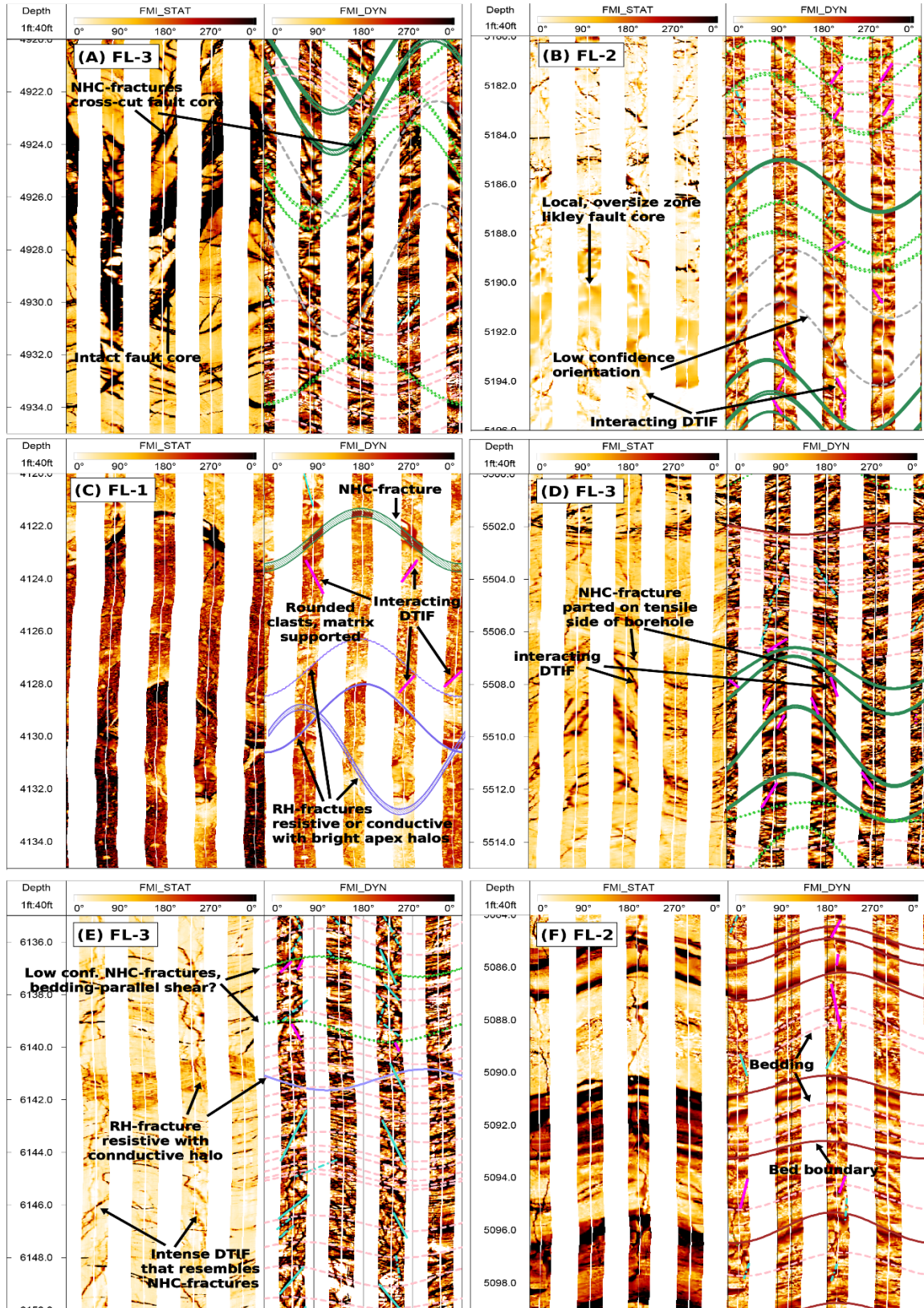


Figure 2: Examples of features from the Fish Lake MBI, with both static (FMI_STAT) and dynamic (FMI_DYN) normalized images.

Luthi and Souhathié (1990) acknowledged that the modelled range of fracture apertures and resistivities were not sufficient, and that there may be issues if their approach is applied to higher-angle fractures. These methodological issues are exasperated in a conventional geothermal setting because, when compared to the sedimentary basin environments for which the excess current approach was developed, these resources have (1) exotic rocks and mineral fills that may influence excess current and (2) common high-angle fractures. For these reasons, we elected not to use the excess current method for determining fracture aperture.

Tectonic stress will localize onto the borehole wall and form hoop stresses that have relatively compressive and tensile areas, as described by the Kirsch solution (Jaeger et al., 2007). When these hoop stresses exceeded the compressive or tensile rock strength, they generate drilling induced damage in the form of borehole breakout (compressive failure) or tensile fractures (tensile fractures, DITF). Drilling induced damage is classified in this study by type and confidence. The types of DITF recognized at Fish Lake include: (1) the typical borehole axial and en echelon forms that form opposite-facing pairs on the tensile sides of the borehole (Davatzes & Hickman, 2010) and (2) a novel category of interacting DITF that form on or between geologic features and at a wide range of azimuths. The mechanism forming interacting DITF is currently unclear. They may be a consequence of how hoop stresses are perturbed by thermal stresses or some local variation in the stress tensor, both of which are common features of geothermal wells (Wallis et al., 2020a, McNamara et al., 2015).

2.2 Geometric Sample Bias

To relate the features interpreted from a borehole wall to the reservoir, we must first understand how these data are impacted by geometric sample bias (Wallis et al., 2020a). Feature planes that are perpendicular to a borehole are very likely to be intersected. In contrast, those that are parallel with the borehole are unlikely to be intersected. Terzaghi (1965) indicated that fractures $< 17.5^\circ$ to the borehole (i.e., $\sin\alpha < 0.3$) are rarely sampled. She coined the term ‘blind zone’ for this persistent gap in data (Figure 3). Isogenic contours map the likelihood that a fracture orientation will be intersected by the given well path. These contours are derived using the acute angle between the borehole axis and fracture (α), where $\sin\alpha=0$ is parallel to the well path and $\sin\alpha = 1$ is perpendicular.

Terzaghi (1965) proposed a correction for this issue of geometric sample bias that uses the acute angle (α) between the fracture plane and the borehole axis to generate a weighted fracture distribution:

Equation 1: Terzaghi correction
$$N_w = \frac{N_0}{\sin \alpha},$$

Where N_0 is the original fracture, α is the acute angle between the discontinuity and the well trajectory, and N_w is the weighing used for correction. However, if a fracture is not sampled it is not available for correction. Therefore, as Terzaghi recognized in her paper, this correction cannot counteract the impact of the blind zone.

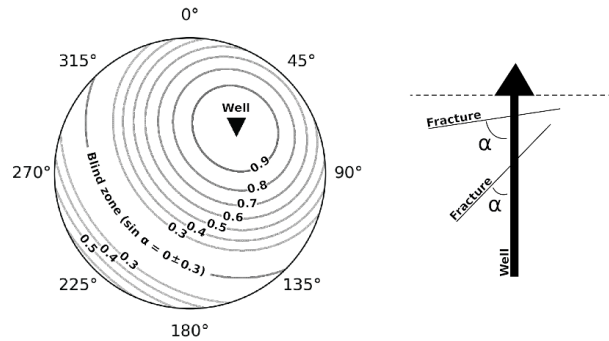


Figure 3: Lower hemisphere, Schmidt stereonet with isogenic contours that map the degree of geometric sample bias for a well inclined 45° to the NE. Figure adapted from Wallis et al. (2020a).

2.3 Stress Quantification

The minimum horizontal stress (S_{hmin}) at Fish Lake was measured using an extended leak-off test (XLOT) in FL-3. The test followed the operational approach described by Wallis et al. (2020b), but it used a modern F-1600 Triplex rig pump. Typically, rig pumps are not used for XLOT because their stroke volume is large (~0.119 bbl per stroke in this case) and they are unable to maintain the low and consistent pump rate required for XLOT (~0.2 bbl/min). Rig pumps are also not positive pressure, so valves must be closed after pumping ceases to prevent backflow and enable monitoring of the pressure decline curve. However, using a modern rig-pump managed with fine operational control from the rig crew can be a cost-effective approach if cement units must be immediately demobilized from site when cementing is complete. Our study illustrates that this approach can generate a reasonable estimate of the fracture gradient.

In a vertical well, the azimuth of the maximum horizontal stress (S_{Hmax}) can be read directly from the azimuth of high confidence DITF. In normal or reverse faulting settings and where horizontal stresses are subequal, the orientation of drilling induced damage on the borehole wall is highly sensitive to the deviation of a borehole > 10° from vertical (Mastin, 1988). Where there is a large difference between the horizontal stresses, the azimuth of DITF is sensitive to borehole inclination, with DITF forming within 10° of S_{Hmax} in wells deviated up to 30° (Mastin, 1988). The magnitude and azimuth of S_{Hmax} in an inclined well can be modelled (Peška & Zoback 1995), provided the pore pressure and the magnitudes of S_{hmin} and the overburden (S_v) are known. 1D geomechanical models have not yet been constructed for the case study wells. We do, however, present a set of theoretical scenarios that explain the observed distribution of DITFs in the case study wells.

2.4 Cuttings Logs

Basic cuttings logs (mud logs) were generated on the wellsite for all three wells and detailed re-logs were conducted post drilling has been completed for FL-1 and FL-2. FL-3 is in progress, so MBI herein are compared to the mud log. The hand-specimen re-log of cuttings focused on separate quantification of primary lithology and secondary alteration, with the greatest interpretation revision arising from those zones with pervasive clay alteration.

Wireline logs and cuttings descriptions are complementary datasets. The cuttings descriptions are depth-corrected using contacts observed in the MBI and the electrofacies. The context provided by detailed geologic description of cuttings informs interpretation of MBI textures. The geologic

context from cuttings analysis also enables more robust inferences about the geologic controls on the fracturing. Finally, integration of MBI and geologic logging allows us to transfer wellbore-scale understanding of controls on permeability to the wider reservoir through the 3D geologic model.

2.5 Electrofacies

Electrofacies is where the variation in electrical log properties is used to classify intervals. In this study, gamma is used as the primary tool to determine electrofacies because it is available in all wells and sensitive to composition. Other available data do, however, contribute to the classification. In all three case study wells, this includes average resistivity from the MBI and caliper. In FL-2, this includes bulk resistivity at various reading depths, borehole compensated sonic, neutron porosity, and density. Care needs to be taken with environmental effects on these logs when generating electrofacies, especially the impact of oversized borehole. Additionally, bound water in hydrothermal clay minerals may significantly distort the neutron porosity log.

2.5 Well Testing

At the time this paper was prepared, a program of well testing was underway to constrain the output capacity of wells and confirm the distribution of feedzones. FL-1 is a historic well drilled in September 1993 and output tested in October 2021. FL-2 and FL-3 were drilled in 2022. Results from injection testing, heating temperature logs, and a short output test are compared in this study to the MBI data. Further testing and interpretation is underway at present.

3. Results of the MBI Interpretation

3.1 MBI Quality

Borehole image quality impacts what features can be interpreted from MBI. Overall, the image quality is pristine (green in Figure 4) with only limited intervals where degraded image quality reduces the number and confidence of features identified (amber) or prevents any interpretation (red). This is most clearly seen at the terminal depth of each log where degraded image quality has reduced our ability to identify fractures or bedding (Figure 4). Image quality is degraded by loss of contact with the borehole wall either due to insufficient pressure applied to tool arms (all pads impacted, caliper smaller than bit size), accumulation of cuttings on the low side (only low-side pads impacted), or oversized borehole (caliper significantly larger than bit size). Tool speed variation that is too great to be resolved by processing, typically referred to as stick-and-pull artifacts, can make an interval of MBI uninterpretable but rarely occurred in these images.

3.1 Depth Distribution of Tectonic Fractures

Together, the three case studies include 5,168 ft (1,575 m) of MBI. Our MBI interpretation identified 1,035 NHC-fractures (Figure 4 and Figure 5). Frequency averaged for the entire logged interval in each well varies from 0.1 to 0.32 fractures per foot. The frequency of NHC-fractures is lower in the Tertiary volcanics and sediments than in the Paleozoic metasedimentary basement. However, the FL-1 results indicate that NHC-fractures in the Tertiary volcanics and sediments are more likely to have larger apparent apertures. Haloed and mineralized fractures are rare in FL-1 and FL-2, and more common in FL-3.

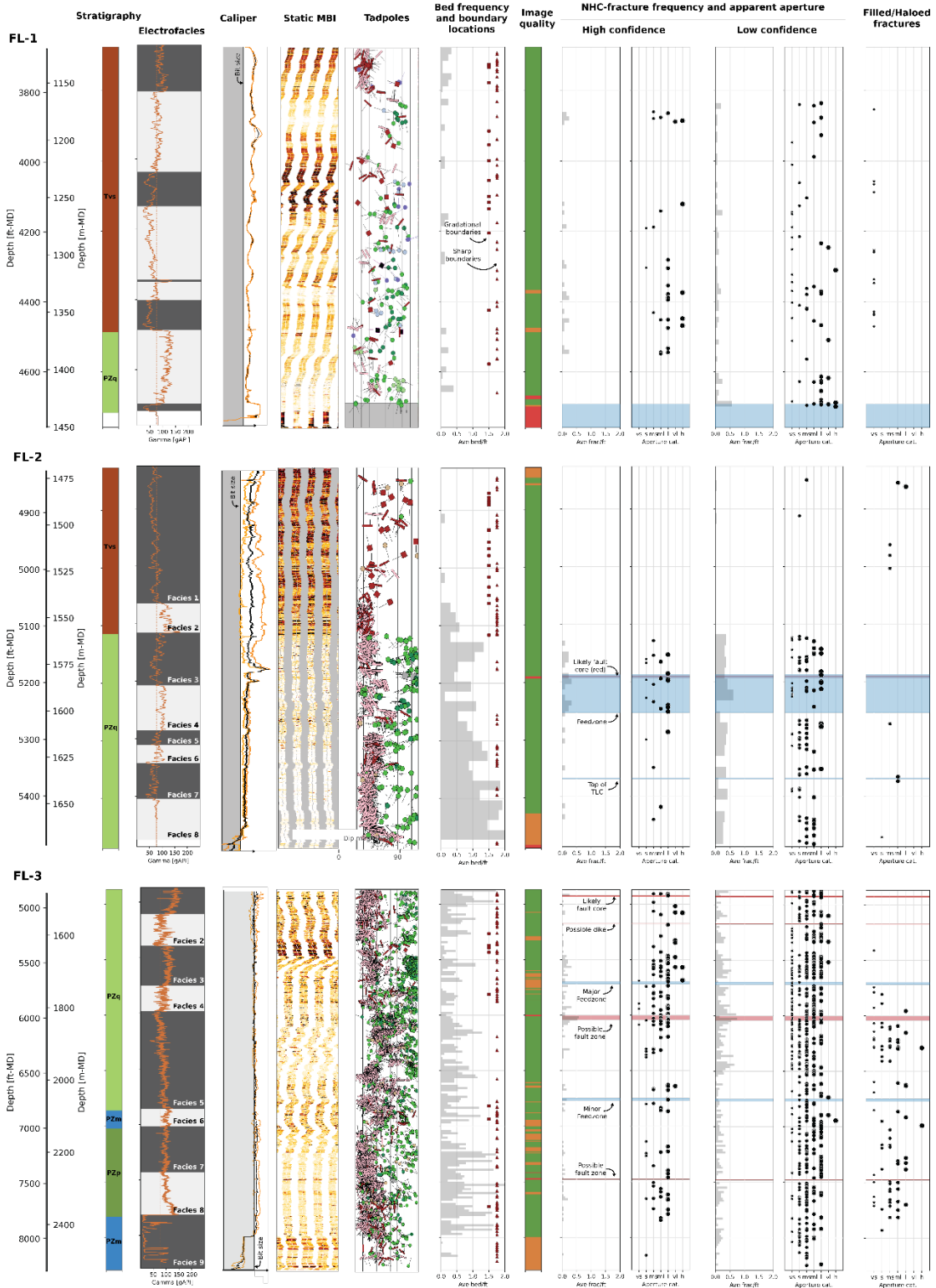


Figure 4: Strip log of the three case study wells with results of MBI interpretation. Frequencies in all cases are the average of a 20 ft interval. Feedzones or other permeability indicators are plotted as blue bars. Depths relative to the drill floor. Formations: Tvs = Tertiary Volcanic Sediments, PZq = Paleozoic Quartzite, PZm = Paleozoic Marble, PZp = Paleozoic Phyllite.

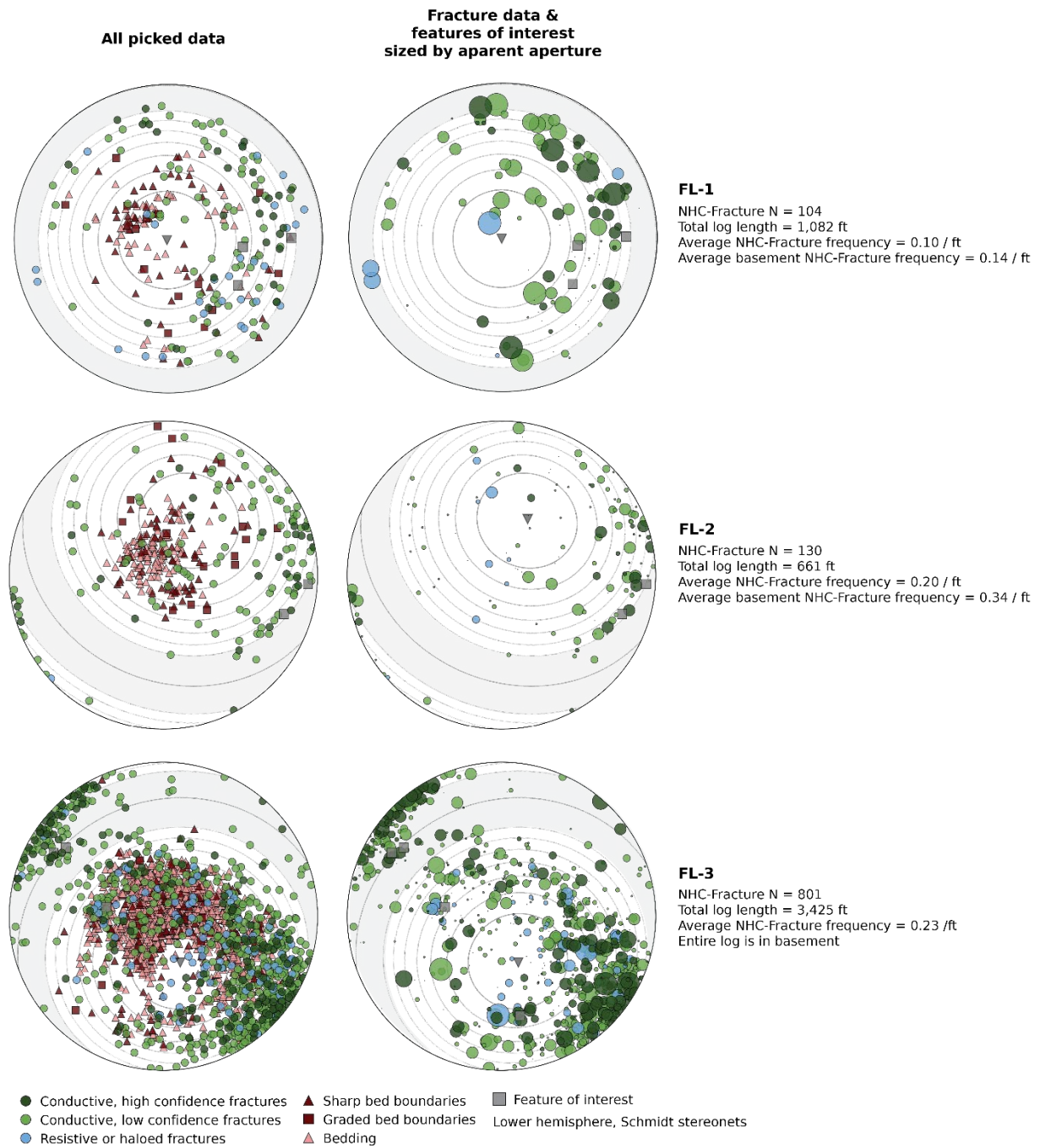


Figure 5: Orientation of features picked in the three MBI case studies. Isogenic contours calculated using the average well deviation and azimuth in the logged interval. The blind zones are shaded grey.

3.2 Orientation of Tectonic Fractures and Geometric Sample Bias

As illustrated by the decision of data relative to the average isogenic contours in Figure 5, all three wells are impacted by geometric sample bias. FL-1 is a vertical well, so high-angle fractures were rarely intersected and, therefore, near absent from the MBI image (Figure 5). The trajectory of wells FL-2 and FL-3 vary in the logged interval (Figure 1), so the location of the blind zone also varies (Figure 6). There is only minor variation in FL-2, so the average isogenic contours are a reasonable approximation. FL-3 has substantial trajectory between the production casing shoe and thermal depth, but most of the logged interval ($\sim 5,250 - 7,600$ ft-MDRF) is well represented by the average.

Because the three Fish Lake wells are drilled in different directions, they have together captured the general structural grain. NHC-fractures most commonly dip E and strike from N-S to ENE-WSW. There is a NE-striking, W-dipping cluster in FL-3 that is exceptional because it is in the blind zone. Given the low probability of the well path intersecting fractures with that orientation, the presence of this cluster in the data indicates numerous NHC-fractures in the reservoir have this trend.

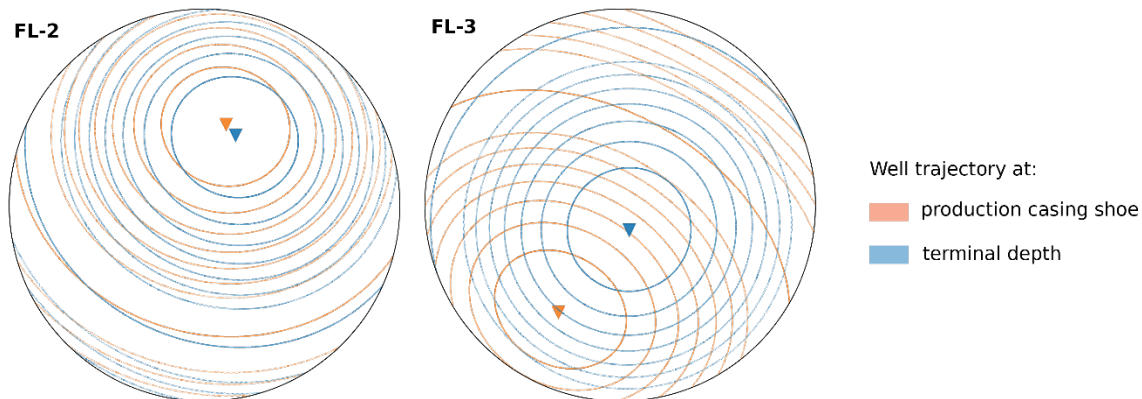


Figure 6: Variation of geometric sample bias for FL-2 and FL-3 in the logged interval.

3.3 Lithology and MBI Textures, Contacts and Bedding

The stratigraphy identified by cuttings analysis in the logged intervals includes Tertiary volcanics and sediments atop a Paleozoic metasedimentary basement that includes quartzite, meta-arkose, phyllite, and marble (Figure 4). The MBI reveal that the Tertiary volcanics and sediments have a wide range of textures and clast sorting (Figure 2). Graded and sharp bed boundaries are common and have a wide range of orientations (Figure 4).

The Paleozoic basement rocks have a comparatively higher frequency of parallel or sub-parallel bedding, but are otherwise almost devoid of texture (i.e., no visible clasts). The attitude and frequency of bedding in the basement varies with lithology. Because it is foliated, phyllite in FL-3 appears to have a very high frequency of bedding (c.f., FL-3, Figure 4). Further detailed analysis of the bed forms is required to determine if systematic trends in bedding attitude seen in the basement at electrofacies 3 and 4 in FL-2 and 4 – 6 in FL-3 are due to the presence of folds or are drag bedding associated with faults.

3.4 Relationship between Lithologic Interpretation and Electrofacies

Our approach to electrofacies captures rock composition variation with depth and we seek to account for any environmental effects that alter log responses. For instance, there is an oversized borehole in the lower half of FL-2 Facies 3 may be responsible for the reduced gamma counts (Figure 4). Consequently, that interval of lower gamma is not classified separately.

The FL-2 case study illustrates how detailed cuttings analysis can explain electrofacies. Electrofacies 3 and 7 had lower average gamma than the rest of the electrofacies within the Paleozoic basement. Detailed cuttings analysis recognized that electrofacies 3 is a quartzite while the remainder of the Paleozoic basement is a feldspar-rich meta-arkose. The low gamma in electrofacies 7 may relate to secondary alteration, as an increase in silica vein material was observed in the cuttings at this depth.

Similarly, electrofacies may highlight where further investigation into the cuttings is needed. At the time this paper was prepared, the detailed re-log of FL-3 had not yet been completed. The mud log identifies two intervals of marble; a thin interval that correlates with Facies 6 and a thicker interval at terminal depth that correlates with Facies 9. These intervals have vastly different gamma responses, where Facies 9 is much lower than 6.

3.5 Fault Identification

Faults were identified during the Fish Lake MBI interpretation using a range of indicators:

- The MBI textures revealed a fault core at FL-3 at ~4,925 ft-MDRF (Figure 2D). Broken, angular resistive blocks that resemble the wall rock are hosted within a conductive, likely clay-rich, matrix.
- Local oversizing with sharp upper and lower surfaces was found in FL-2 at ~5,190 ft-MDRF (Figure 2D). This local oversizing was likely generated by the selective removal of a friable fault core.
- The peak in fracture frequency at 6,000 ft-MDRF in FL-3 (labelled ‘possible fault zone’ in Figure 4) may be due to the presence of a fault damage zone. In the terminal depth of FL-1, the FMI tool at maximum extension does not touch the borehole wall (Figure 4). It is possible that this enlargement is generated by intense fracturing within a fault zone.

In many of the cases above, the fault is not a single sinusoid that can be picked from the image. Even where the fault core is visible, the orientation may be poorly constrained by complexity or damage on the upper and/or lower surfaces. Furthermore, faults may have local variations in their orientation. An MBI may resolve offset of bedding along a surface in the borehole image. However, a fault identified in this manner typically has a small offset (meter to sub-meter) and is unlikely to be hydrologically meaningful. Local and systematic change in bedding dip (drag bedding) may reveal the presence of a fault. However, the complex fold history of the Paleozoic basement precludes confident use of this fault identification approach.

Petrophysical logs can be used to corroborate the presence of a fault where there is a well-developed fault core or where lithologies with discernibly different compositions are juxtaposed. FL-2 is the only one of the three wells to have petrophysical logs beyond the basic gamma. These

logs corroborate the presence of a fault core at ~5,191 ft-MDRF (Figure 8, marked A). This is a zone of low density and slow velocity is consistent with presence of clay. The neutron porosity is also high, which may be due to water bound in the clays rather than free water in pore spaces. The presence of oversized borehole can impact petrophysical log response. However, the minimal density, sonic, and neutron porosity log response to a more oversized interval above the fault supports our conclusion that log responses in the fault zone are real.

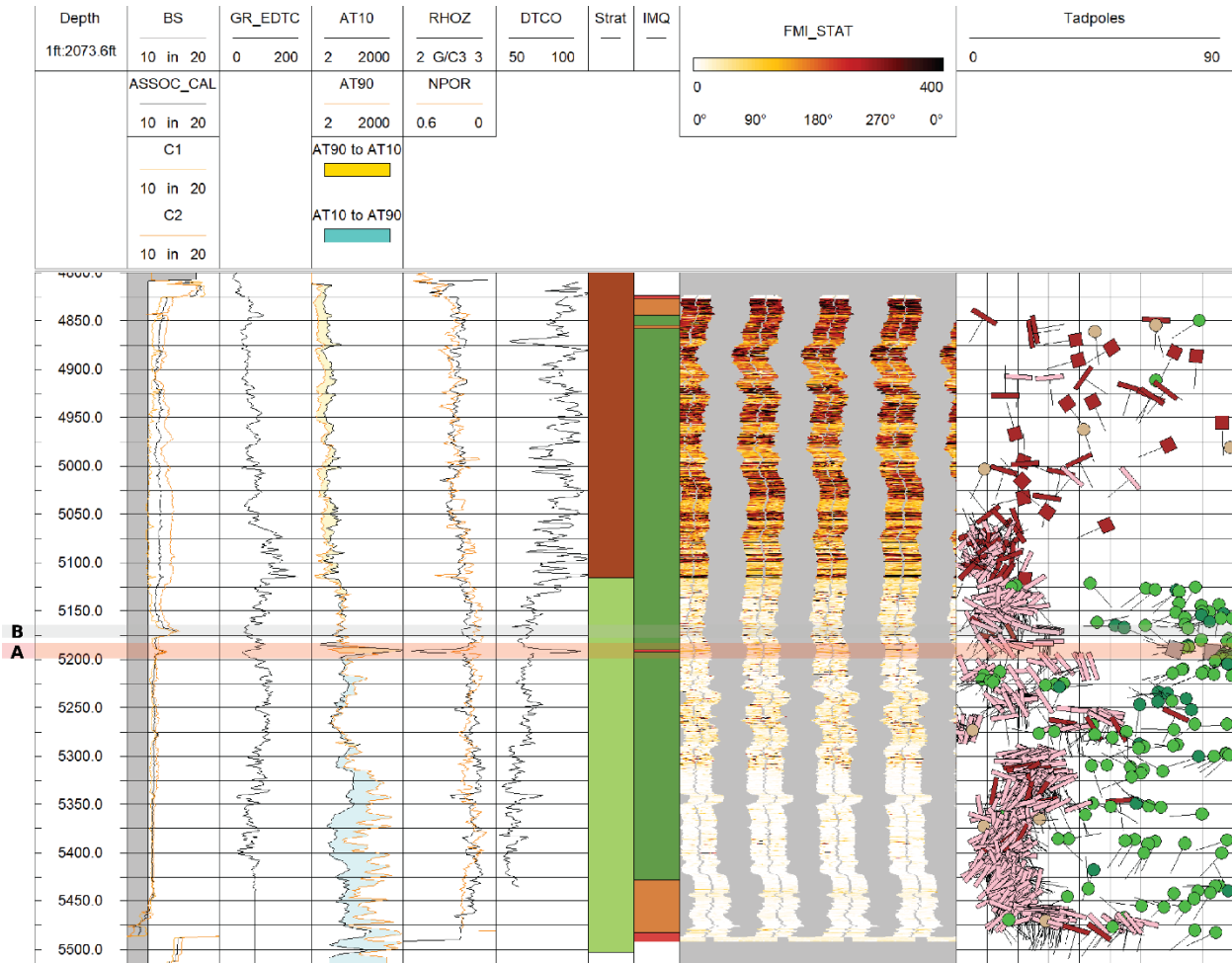


Figure 7: Petrophysical indicators of fault in FL-2. Identified fault (A) and oversized borehole for comparison (B). Title codes: Borehole size BS, associated caliper ASSOC_CAL, x or y direction caliper C1 C2, gamma ray GR_EDTC, shallow resistivity AT10, deep resistivity AT90, density RHOZ, neutron porosity NPOR, borehole compensated sonic DTCO, stratigraphy Strat, image quality IMQ, and statically normalized image FMI_STAT.

3.6 Distribution of Drilling Induced Damage

Quantification of drilling induced damage was impacted by spaces between the pads (Figure 7). Gaps in determinations are generated when the tensile side of the borehole is between pads (e.g., 4,200 – 42,50 ft-MDRF in FL-1). However, given the four arms and ample borehole coverage (~54%), these images quantify the distribution of drilling induced damage reasonably well.

There is no borehole breakout in the Fish Lake wells. There are, however, many instances of DITF. The frequency of DITF correlates with stratigraphy. There is a lower frequency of DITF in the Tertiary volcanics and sediments than in the Paleozoic basement rocks. The distribution of interacting DITF is particularly uneven with depth. For instance, in FL-2 there are peaks in the frequency of interacting DITF that are more than twice the background rate at the Tertiary to Paleozoic unconformity (~5,120 ft-MDRF), coincident with the fault zone (~5,190 ft-MDRF), and at ~5,330 ft-MDRF. There is nothing clearly distinctive in the MBI, in terms of other fault zone indicators or lithologic transitions, coincident with the deepest frequency peak.

The type and azimuth of DITF is influenced by borehole deviation. Most DITF in the vertical well (FL-1) are axial. In contrast, the two deviated boreholes (FL-2 and FL-3) are dominated by en echelon DITF. The trajectory of FL-3 changes significantly in the logged interval, with most change in azimuth above 5,500 ft-MDRF. At the casing shoe, FL-3 DITF are located on the high- and low-side of the borehole (0 and 180 deg-LS). By 5,500 ft-MDRF, DITF are forming on the left and right sides of the borehole (90 and 270 deg-LS).

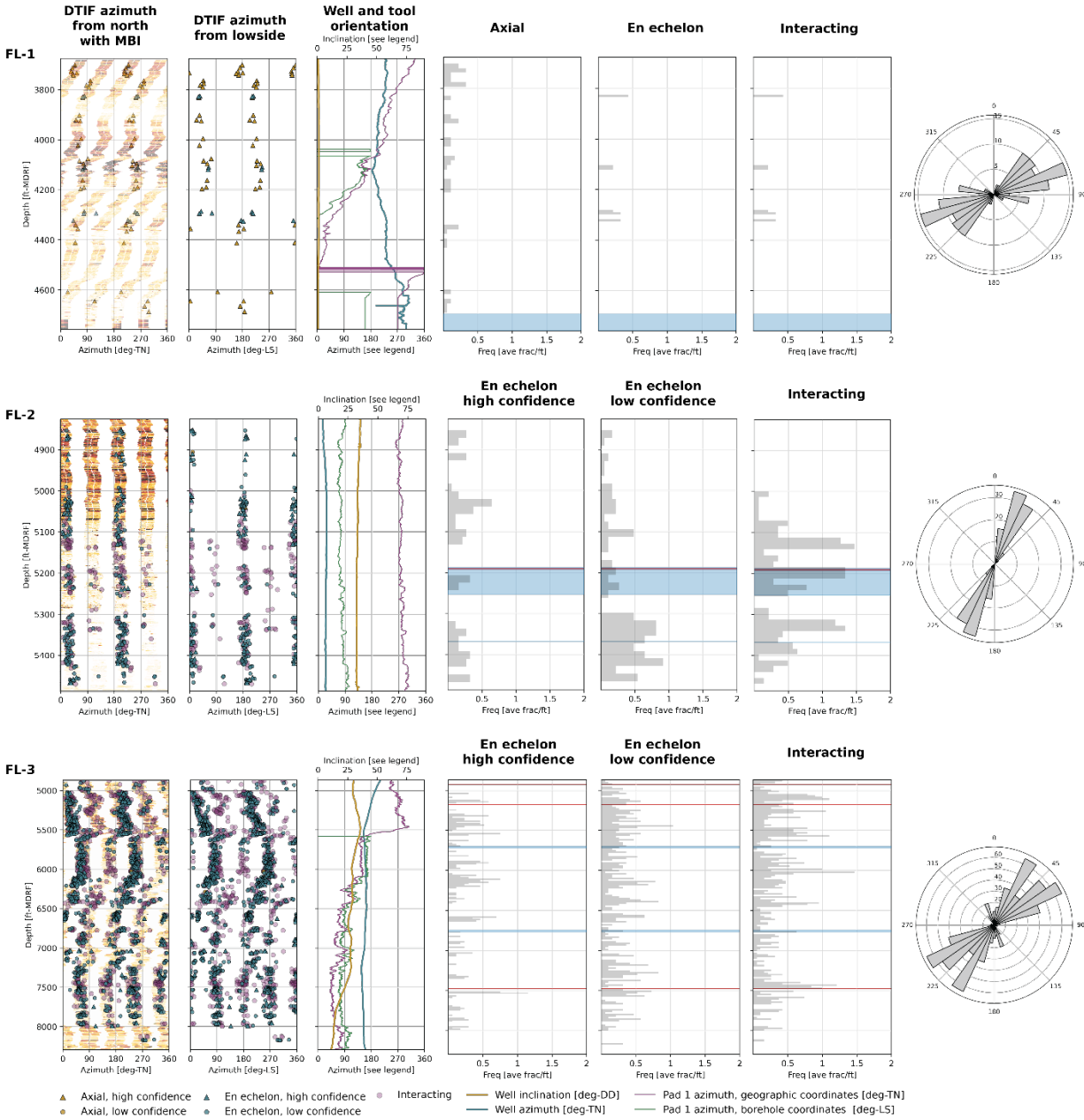


Figure 8: Mid-point of DITF plotted by depth. Average frequency calculated for 20 ft intervals. There is no axial DITF frequency plot for FL-2 and FL-3 because they are too rare. Feedzones and other permeability indicators are plotted as blue bars. Possible faults and dike in FL-3 are plotted as red bars. Rose diagrams are radially symmetric and only include high-confidence axial or en echelon DITF.

3.6 XLOT Data and Interpretation

The XLOT test in FL-3 yielded a fracture gradient of 0.59 – 0.62 psi/ft, with the fracture propagation pressure at the wellhead and pump used to generate the estimate range (Figure 9). The strokes are visible in the undulating pressure recorded by the pump pressure gauge, but this variation is more muted in the wellhead pressure sensor data. Both cycles reached the same fracture propagation pressure. The increase in pump rate, and associated peak in pump pressure, at the end of cycle 1 is excluded from this analysis.

Because of the operational conditions, the fracture propagation pressure is the most reliable measure of the fracture gradient. The pressure incline at the start of each cycle varies in response to fluctuations in pump rate (1 – 3 strokes/min or 0.117 – 0.351 bbl/min), so the leak-off point or fracture re-opening pressure cannot be accurately identified. The instantaneous shut-in pressure and fracture closure pressure cannot be confidently interpreted because rig pumps are not positive pressure. The need to rely on the fracture propagation pressure as the best measure in adverse operational conditions highlights the importance of pumping two barrels after pressure has plateaued.

This is the first measurement of the fracture gradient at Fish Lake. Given that the structural setting is likely to be normal or transitional to strike slip, this fracture gradient would correlate with the magnitude of the minimum horizontal stress. Although the uncertainty range of the XLOT result seems large, it is within the 0.05 psi/ft range expected for multiple XLOT within a single geothermal resource (Wallis et al., 2020b). Future testing will improve our understanding of stress magnitude and its variation at Fish Lake.

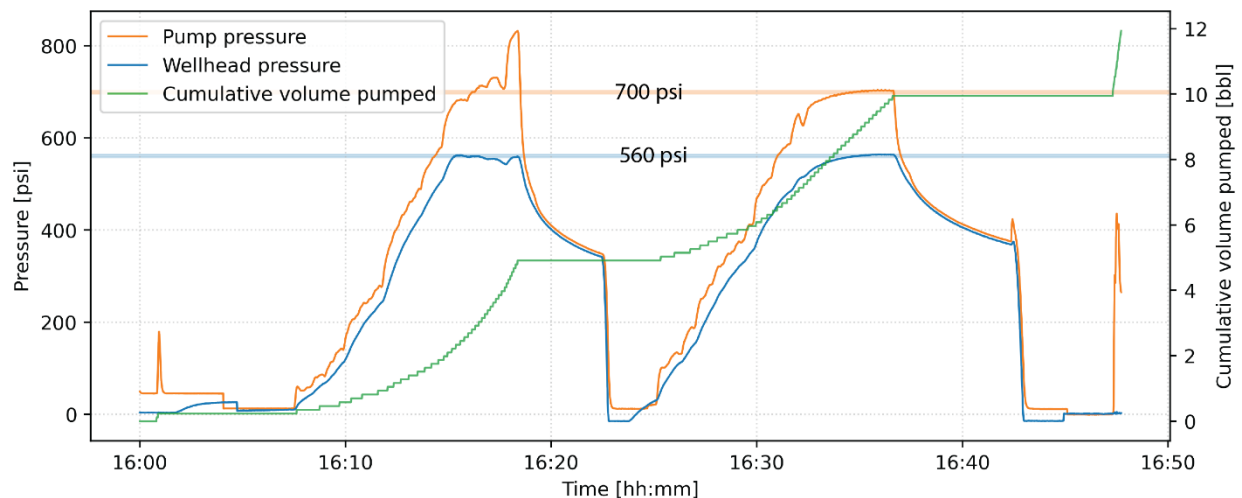


Figure 9: XLOT test pressure-time history plot for test conducted at 4,565 ft-VDRF casing shoe with 9 ppq fluid (watered-back mud), with the range of fracture propagation pressure's highlighted.

4. Discussion

4.1 Rotation of DITF on Borehole wall

Our MBI interpretation of the three Fish Lake wells revealed that the azimuth of DITF systematically varies with borehole deviation (Figure 8). To explore this phenomenon, we generated a range of model scenarios that describe tectonic stress resolves onto an inclined borehole (Peška and Zoback, 1995). The scenarios forecast the azimuth DITF on the borehole wall in each of three stress settings, with a N-S azimuth of S_{Hmax} in all cases, and a range of borehole inclination and azimuth (Figure 10). Note that the DITF azimuth is plotted in borehole coordinates, clockwise from the low side.

The azimuth of DITF in geographic coordinates can be directly read as the azimuth of S_{Hmax} (Mastin, 1988; Peška and Zoback, 1995). In contrast, the formation of DITF on the wall of a deviated is sensitive to the magnitude and azimuth of all components of the stress tensor. The tilt of DITF also progresses from borehole axial to en echelon as the well is deviated (Peška and Zoback, 1995), which is observed in the Fish Lake wells.

The unit slope (black) in Figure 10 is a near-vertical well. It illustrates how the azimuth of DITF tracks around the borehole wall as the direction of deviation is changed. In essence, this unit slope shows that the azimuth of DITF in geographic coordinates remains the same but is changing in borehole coordinates as the borehole azimuth changes. Any variation away from this unit slope is where the azimuth of DITF in geographic coordinates will no longer align to the azimuth of S_{Hmax} .

Variation of scenario results away from the unit slope in Figure 10 illustrates how DITF azimuth is more sensitive to borehole inclination/azimuth in a normal faulting setting than in a strike slip setting. Sensitivity is further increased in cases where S_v is much greater than the horizontal stresses. The DITF azimuth is more likely to align with the S_{Hmax} azimuth when the borehole is deviated parallel to that stress direction.

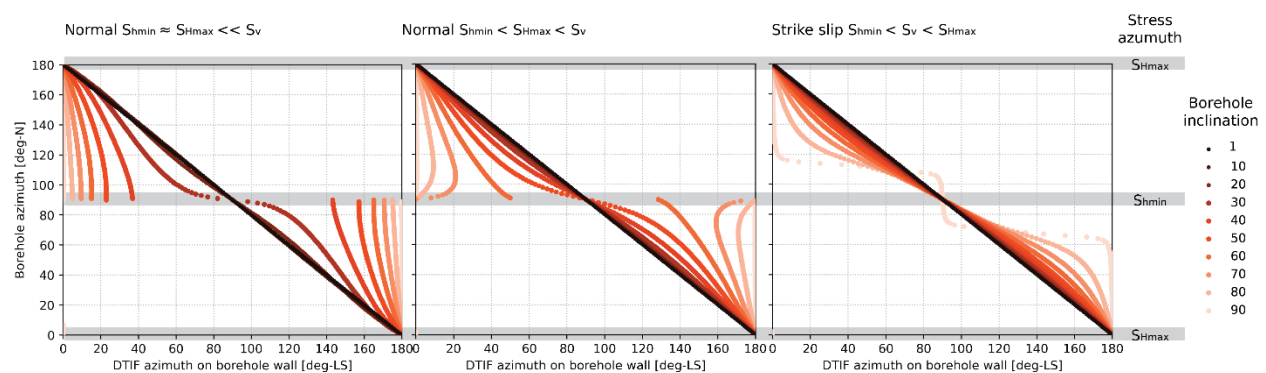


Figure 10: Model scenarios for three stress cases that forecast the location of DITF on the borehole wall, given a N-S azimuth of S_{Hmax} and a range of borehole inclination and azimuth. DITF azimuth is in degrees clockwise from the low side of the borehole (deg-LS).

These observations explain the pattern of DITF observed in Fish Lake wells (Figure 8). DITF in FL-1 track around the borehole wall in alignment with the azimuth of S_{Hmax} , while the two deviated wells are impacted by the full stress tensor. DITF in FL-2 forms on the low and high-side of the borehole, consistent with a borehole azimuth that is sub-parallel to S_{Hmax} . At the production casing shoe, FL-3 is also sub-parallel to S_{Hmax} and DITF are around the low and high sides of the borehole. However, the borehole azimuth turns with depth. Subsequently, the position of DITF track from the low and high side of the borehole to the left and right. Given the magnitude of DITF azimuth variation we observe in FL-3, Fish Lake is more likely to be a normal faulting setting than strike slip. However, further geomechanical modelling is required to confirm this.

4.2 Controls on Wellbore-Scale Permeability at Fish Lake

The completed and, for FL-3 provisional, well testing reveals that the Fish Lake wells are good producers. FL-1 has a productivity index (PI) of ~ 18 t/hr/bar, while FL-2 has an injectivity index of 65 t/hr/bar and PI of 72 t/hr/bar. Early results for FL-3 indicate this well has a capacity around 70% of FL-2. Feedzone depths from well testing are indicated in Figure 4.

Wallis (2023) evaluated MBI against the well test results in seven wells from five high-temperature, volcanic-hosted geothermal systems. These wells had an injectivity index that ranged between 3 and > 500 t/hr/bar. The study revealed a relationship between total well capacity and the average frequency of NHC-fractures: The two cases with a well capacity above P10 for geothermal wells (i.e., with an II > 51.5 t/hr/bar; Grant, 2008) had an average NHC-fracture frequency 2 – 3 times greater than the other three case studies. This frequency in high-capacity wells was 1.98 and 2.15 fractures per meter (0.57 and 0.66 fractures per foot) and the lower capacity wells ranged from 0.44 to 0.87 fractures per meter (0.13 to 0.27 fractures per foot).

Wells at Fish Lake do not conform to the capacity to average fracture frequency relationship observed by Wallis (2023) in volcanic-hosted geothermal wells. FL-2 has an injectivity above the P10 defined by Grant (2008), but it has a fracture frequency that aligns with lower capacity volcanic-hosted geothermal wells. This difference may relate to the contrast in reservoir-scale fluid flow. The volcanic-hosted systems in Wallis (2023) comprise great thicknesses of isothermal temperatures, indicating broad advection through a fracture network and each well had 4 – 9 feedzones. In contrast, deep circulation systems like Fish Lake have narrower intervals of near-isothermal temperatures where advection is localized within geological features. They also have fewer, and typically narrower, feedzones than their volcanic-hosted counterparts. Consequently, averaging fracture frequency over an open-hole length at Fish Lake does not generate a fair comparison to the volcanic-hosted cases. Around feedzones in the Fish Lake wells, NHC-fracture frequency peaks that are > 0.5 fractures per foot, which is comparable to overall average frequency in high-capacity, volcanic-hosted wells.

Feedzones identified using flowing pressure, temperature and spinner logs acquired under injection or production are the best and most direct measure of fluid flux, especially where the interpretation of those logs is supported by static temperature data acquired as the well heats. However, testing at a single flow rate or direction (injection/production) may not capture the details of well-scale permeability. Feedzones may vary in magnitude or even location depending on the pressure difference between the wellbore and reservoir. For instance, injection into or production from a large capacity feedzone, like what is observed in FL-2, may mask smaller feedzones. The presence of a perforated liner can make feedzones appear wider, shallower, and

merge small discrete feedzones into a single zone (Goble and McLean, 2020). Given that the three Fish Lake wells discussed in this study are tested barefoot, the feedzone depth is likely to be a good indicator of the actual depth of permeability.

Comparison between the depth of feedzones and the MBI interpretation reveals two key insights into what controls wellbore scale permeability:

- The variation of mechanical rock properties due to lithology and/or alteration appears to influence the distribution of permeability. No feedzones have been identified in the Tertiary volcanics and sediments. The MBI revealed this formation to have few fractures. Relative to the Paleozoic basement, the Tertiary volcanics are also conductive. This may indicate a higher proportion of clay and go some way to explain the lack of brittle failure.
- Some feedzones are hosted by faults, but not all the faults are feedzones. There is a single feedzone identified by well testing in FL-2 and this is coincident with the fault at ~5,190 ft-MDRF. Interestingly, there were no significant drilling fluid losses in this zone and the well did not experience total loss circulation until drilling reached 5,368 ft-MDRF, some 114 feet below the fault. Although the well testing program in FL-3 is not yet complete, the provisional results show no indication of a feedzone at the ~4,925 ft-MDRF fault.

One of the differences between the permeable faults and likely non-permeable faults in FL-2 and FL-3, respectively, is the abundance of interacting DITF (Figure 7). The fault at FL-2 coincides with a sharp increase in interacting DITF while the FL-3 fault has far fewer of these features. In their study of high-temperature, volcanic-hosted geothermal wells, Wallis (2023) found that three quarters of the feedzones correlate with interacting DITF. A similar correlation between permeability and interacting DITF appears to be present at Fish Lake.

5. Conclusions

Our study demonstrated how integrated analysis of well testing, geology, and MBI interpretation yields insight into the controls on wellbore-scale permeability. Understanding these controls will inform future well targets and the reservoir conceptual model. At Fish Lake, the variation of rock mechanical properties and the distribution of faults influence permeability. However, not all faults identified in the MBI were permeable. The interacting-type DITF may be a useful diagnostic criterion for discerning which faults are permeable. Average fracture frequency in Fish Lake wells were found to be lower than volcanic-hosted geothermal wells with a similar capacity. Differences in reservoir-scale fluid flow in deep-circulation and volcanic geothermal systems may be the source of this contrast.

We described an innovative and cost-effective approach to XLOT testing, where a rig pump was used. This generated a reasonable result and, along with drilling induced damage interpreted from the MBI, is important data for constraining the stress tensor (Rogers et al., 2023). We observed that DITF azimuth varies between vertical and inclined wells, and then presented a set of model scenarios that explain this variation. Future work can apply these key data to constraining the stress tensor and, subsequently, determine the stress sensitivity (i.e., likelihood of being open to flow) of individual fractures and reservoir-scale faults (Barton et al., 1998).

Acknowledgement

The authors thank Open Mountain Energy for permission to publish this work. We also acknowledge the open-source Python ecosystem, including the package `fractoolbox` which was used to generate isogenic contours and model stress (<https://github.com/ICWallis/fractoolbox>).

REFERENCES

- Barton, C. A., Zoback, M. D., & Moos, D. (1995). Fluid flow along potentially active faults in crystalline rock. *Geology*, *23*, 683–686.
- Barton, C. A., Hickman, S. H., Morin, R., Zoback, M. D., & Benoit, D. (1998). Reservoir-scale fracture permeability in the Dixie Valley, Nevada, geothermal field. *Proceedings, Workshop on Geothermal Reservoir Engineering, Stanford, California*, 315–322.
- Davatzes, N. C., & Hickman, S. H. (2010). Stress, fracture, and fluid-flow analysis using acoustic and electrical image logs in hot fractured granites of the Coso Geothermal Field, California, U.S.A. In C. Pöppelreiter, C. García-Carballido, & M. Kraaijveld (Eds.), *Dipmeter and Borehole Image Log Technology* (pp. 159–293).
- Goble, I., & McLean, K. (2020). Accurate location of feed zones: Assessing obscuration by the liner in geothermal wells. *Proceedings, New Zealand Geothermal Workshop*.
- Grant, M. A. (2008). Decision Tree Analysis of Possible Drilling Outcomes to Optimise Drilling Decisions. *Proceedings, Workshop on Geothermal Reservoir Engineering*. Stanford, California.
- Jaeger, J. C., Cook, N. G. W., & Zimmerman, R. W. (2007). *Fundamentals of Rock Mechanics: Vol. 4th Edition*. Blackwell Publishing.
- Luthi, S. M., & Souhaite, P. (1990). Fracture apertures from electrical borehole scans. *Geophysics*, *55*(7), 821–833.
- Massiot, C., McNamara, D. D., & Lewis, B. (2015). Processing and analysis of high temperature geothermal acoustic borehole image logs in the Taupo Volcanic Zone, New Zealand. *Geothermics*, *53*, 190–201.
- McNamara, D. D., Massiot, C., Lewis, B., & Wallis, I. C. (2015). Heterogeneity of structure and stress in the Rotokawa Geothermal Field, New Zealand. *Journal of Geophysical Research: Solid Earth*, *120*(2), 1243–1262.
- McNamara, D. D., Milicich, S. D., Massiot, C., Villamor, P., McLean, K., Sépulveda, F., & Ries, W. F. (2019). Tectonic Controls on Taupo Volcanic Zone Geothermal Expression: Insights from Te Mihi, Wairakei Geothermal Field. *Tectonics*, *38*(8), 3011–3033.
- Mastin, L. (1988). Effect of borehole deviation on breakout orientations. *Journal of Geophysical Research: Solid Earth*, *93*(B8), 9187–9195.

- Nemčok, M., Moore, J. N., Christensen, C., Allis, R., Powell, T., Murray, B., & Nash, G. (2007). Controls on the Karaha–Telaga Bodas geothermal reservoir, Indonesia. *Geothermics*, 36(1), 9–46.
- Peška, P., & Zoback, M. D. (1995). Compressive and tensile failure of inclined well bores and determination of in situ stress and rock strength. *Journal of Geophysical Research: Solid Earth*, 100(B7), 12791–12811.
- Rogers, A., Wallis, I.C., Fox, A. (2023, this volume) A comparison of pre-drill and post-drill in-situ stress estimates for the Eavor-Deep™ 18,000 ft-TVD closed-loop geothermal demonstration well. *GRC Transactions, Vol. 47*.
- Robinson, P. T., & Crowder, D. F. (1973). Geologic map of the Davis Mountain Quadrangle, Esmeralda and Mineral Counties, Nevada, and Mono County, California (No. 1078).
- Sone, H., Mudatsir, O., Jin, Z., Folsom, M., Ramirez, G., & Feigl, K. L. (2023). WHOLESCALE - Characterization of Conductive Fractured Zones Based on Borehole Data at San Emidio Geothermal Field, Nevada. *Proceedings, Workshop on Geothermal Reservoir Engineering*. Stanford, California.
- Terzaghi, R. D. (1965). Sources of error in joint surveys. *Geotechnique*, 15(3), 287–304.
- Wallis, I. C., McNamara, D., Rowland, J. V., & Massiot, C. (2012). The nature of fracture permeability in the Basement Greywacke at Kawerau Geothermal Field, New Zealand. *Proceedings, Workshop on Geothermal Reservoir Engineering*. Stanford, California.
- Wallis, I. C., Rowland, J., Dempsey, D., Allan, G., Sidik, R., Martikno, R., McLean, K., Sihotang, M., Azis, H., & Baroek, M., (2020a). Approaches to imaging feedzone diversity with case studies from Sumatra, Indonesia and the Taupo Volcanic Zone, New Zealand. *Proceedings, New Zealand Geothermal Workshop*.
- Wallis, I. C., Pye, D. S., Dempsey, D. E., & Rowland, J. V. (2020b). A users guide to leak-off test procedures and interpretation for geothermal wells. *Proceedings World Geothermal Congress 2020+1*.
- Wallis, I. C., (2023). The geologic controls on geothermal fluid flux at the district-, reservoir, and wellbore scale. Unpublished PhD Thesis, University of Auckland.